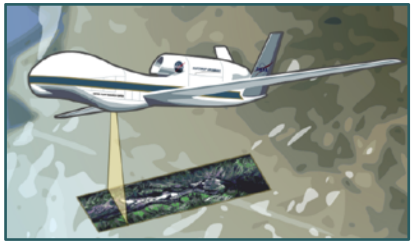

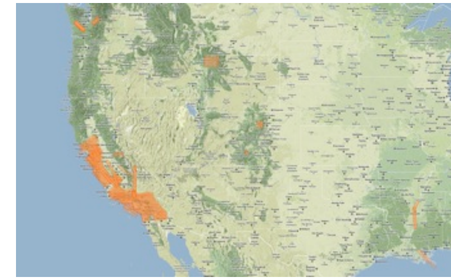

Status on UAVSAR
Future Directions

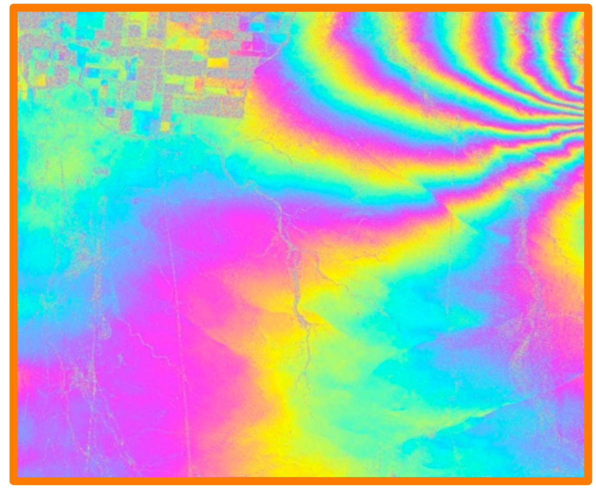

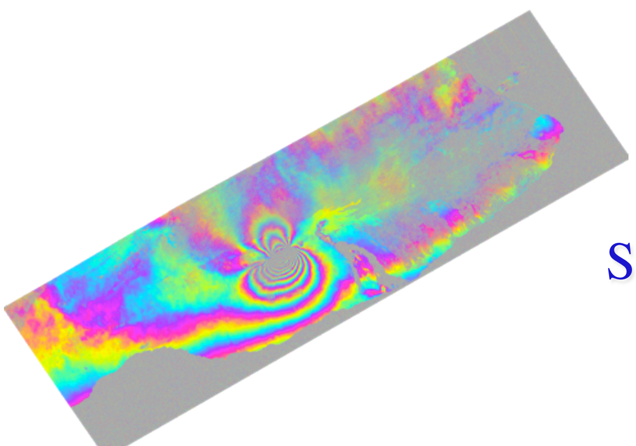

by

Scott Hensley and Yunling Lou

UAVSAR Workshop

October 16, 2015

UAVSAR Evolution

- It is now more than a decade since the beginning of the UAVSAR program and the question is in what direction(s) should the system evolve.
- UAVSAR continues to expand its capabilities in several directions that include:
  - Multi-squint mode
  - Bistatic Observations
  - Circular Trajectories and spotlight modes
  - Increased bandwidth and sampling frequency
  - Single-pass L-band interferometry (on Global Hawk)
  - Tomography
- We are also interested in other ideas or experiments that can be conducted with a minimal amount of hardware and flight hours that can expand the capabilities or range of applications of the UAVSAR system.

Multi-Squint

Multi-Squint Observations

- Vector deformation measurements using differential radar interferometry can normally only be obtained by acquiring multiple repeat pass acquisitions from different vantages.
- This prompts one to ask:
  - Is there a way to obtain the full vector deformation using a single repeat pass?
  - Can we estimate something about the tropospheric delay term?
- UAVSAR has the ability to acquire data simultaneously at multiple squint angles thus opening the possibility of obtaining vector deformation measurements.
- Multi-squint interferometric observations my potentially be used to obtain additional vegetation structure measurements.
  - Verify azimuth symmetry assumptions for flat terrain
  - Provide additional vantages over azimuthally sloped terrain
  - Some k_z diversity

UAVSAR Data Acquisition Modes

Strip Mode SAR

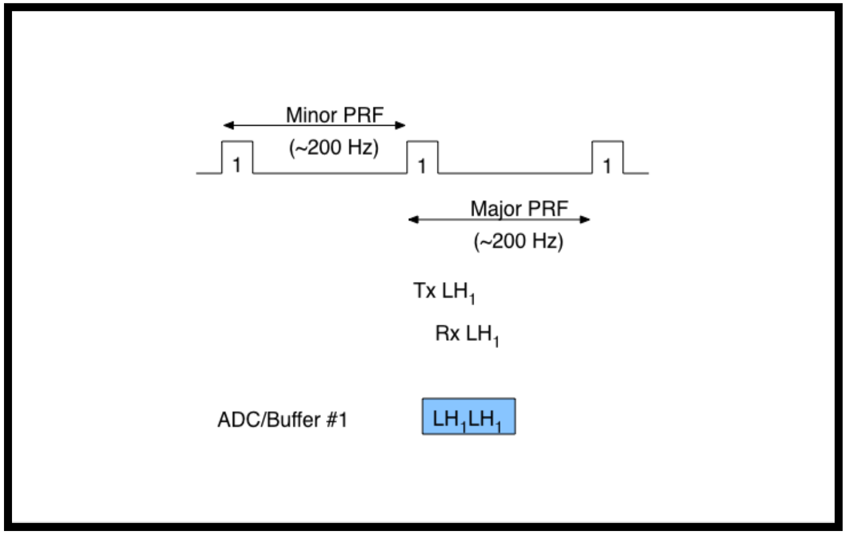

Polarimetric SAR

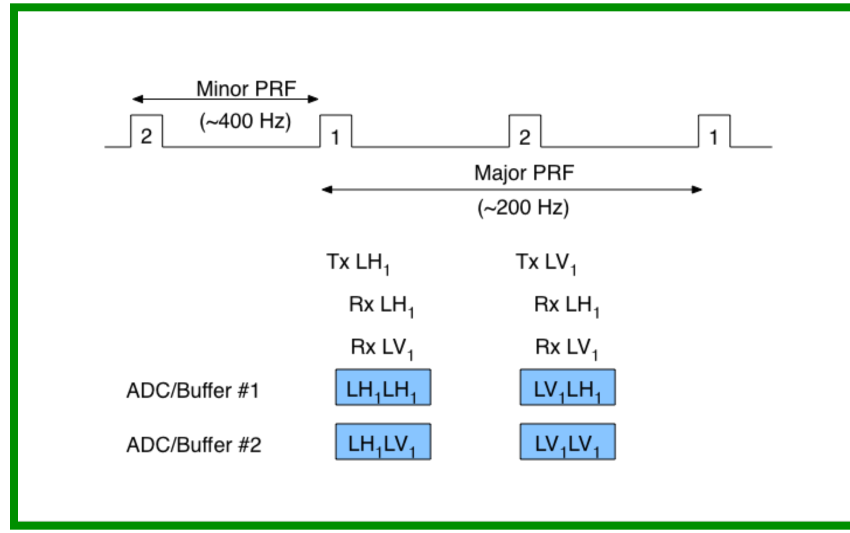

Multi Squint Vector Deformation

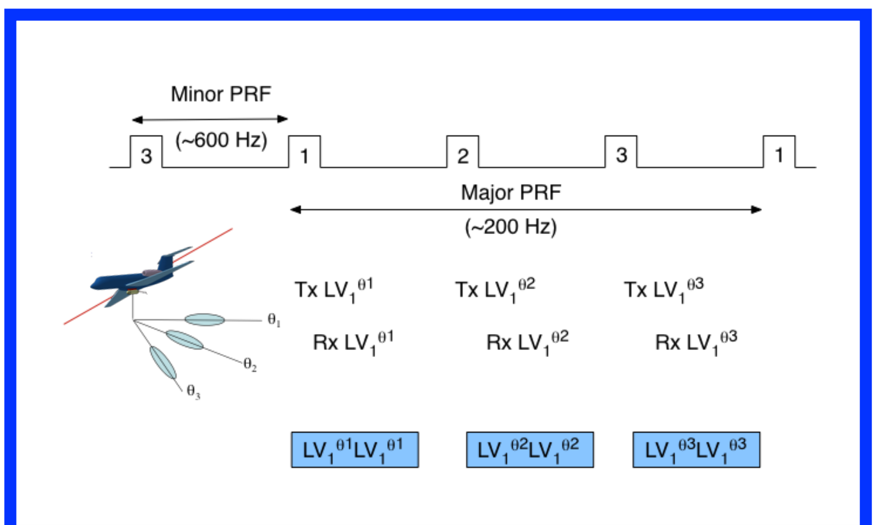

CoPol Monopulse

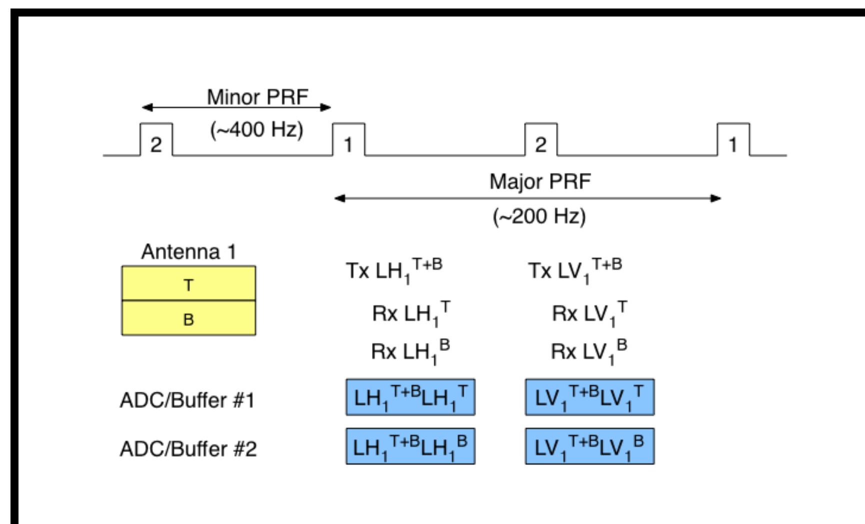

Differential Phase Measurement

- The differential interferometric phase measurement is given by

$$\phi = \frac{4\pi}{\lambda}\left[-\langle\vec{b},\hat{\ell}\rangle + \langle\vec{d},\hat{\ell}\rangle + \Delta\rho_{atm}\right] + \phi_{noise}$$

Topography Term — **Change Term** — **Atmosphere Term**

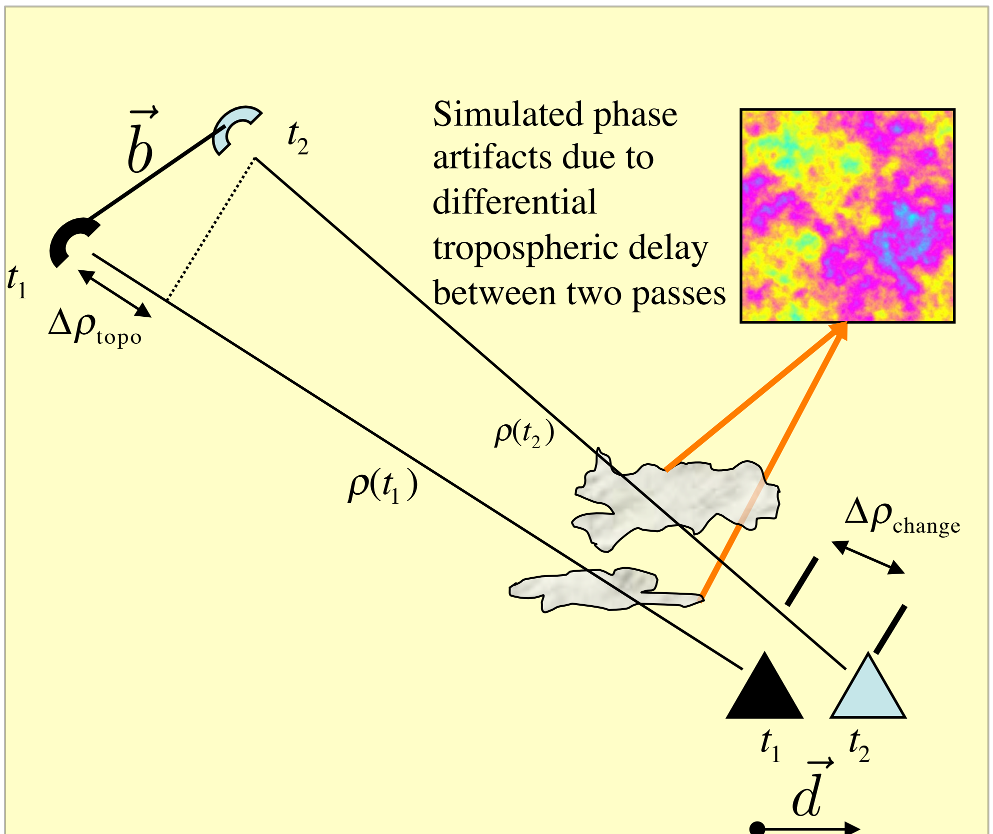

- Topography term is assumed known and removed for remainder of discussion
- Measurement only of surface displacement along line-of-sight that can not be distinguished from tropospheric path delay
- Tropospheric path delays cause artifacts in repeat-pass interferometric synthetic aperture radar (InSAR) measurements of surface displacement
  - Rapidly varying tropospheric delays (both spatially and temporally) are most problematic
  - Such variations are primarily due to changes in water vapor content along signal propagation path

Multi-Squint Geometry

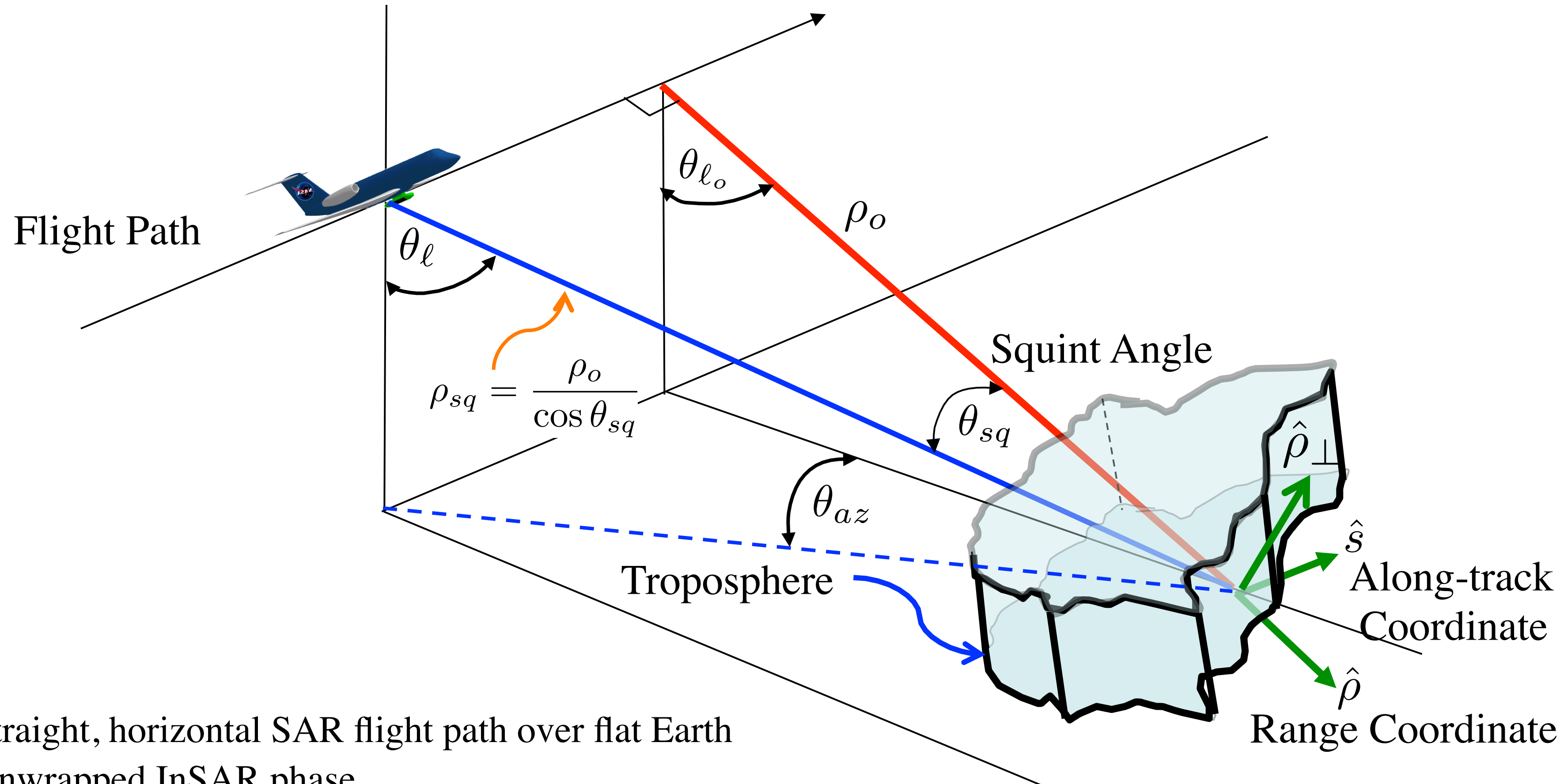

- Straight, horizontal SAR flight path over flat Earth
- Unwrapped InSAR phase
- Thin-layer troposphere just above ground surface
- Ideal conditions:
  - Good interferometric correlation
  - No ionospheric effects
  - Perfectly repeating flight path
- Work in slant-plane (ρ,s) coordinate system

$$\vec{d} = \begin{bmatrix} d_\rho & d_s & d_\perp \end{bmatrix}$$

$$\begin{aligned} \phi &= \frac{4\pi}{\lambda}\left[\langle \vec{d}, \hat{\ell}\rangle + \Delta\rho_{atm}\right] + \phi_{noise} \\ &= \frac{4\pi}{\lambda}\left[d_\rho \cos\theta_{sq} + d_s \sin\theta_{sq} + \frac{\Delta\rho_{\mathrm{atmbroadside}}}{\cos\theta_{sq}}\right] + \phi_{noise} \end{aligned}$$

Subsidence Model

- To test the inversion we simulated a subsidence bowl with 10 cm of vertical displacement and 5 cm of radially inward lateral displacement.
- For the atmosphere we assumed a simple -8/3 power law PSD with 0 mean and a 2 cm standard deviation.

Parameter	Value
Flank Radius (r_f)	1.5 km
Bowl Radius (r_b)	10 km
Lateral Displacement (L_m)	5 cm
Steepness Factor (s_f)	2.3
Vertical Rim (u_t)	0
Vertical Center (u_b)	-10 cm

$$\vec{d}_{enu} = \begin{bmatrix} -L_m \sin\left[\frac{\pi(e-e_o)}{r_b}\right] \\ -L_m \sin\left[\frac{\pi(n-n_o)}{r_b}\right] \\ \frac{(u_t-u_b)}{2\tanh s_f}\tanh\left[\frac{2s_f(r-r_f)}{r_b-r_f} - s_f\right]\frac{u_t+u_b}{2} \end{bmatrix}$$

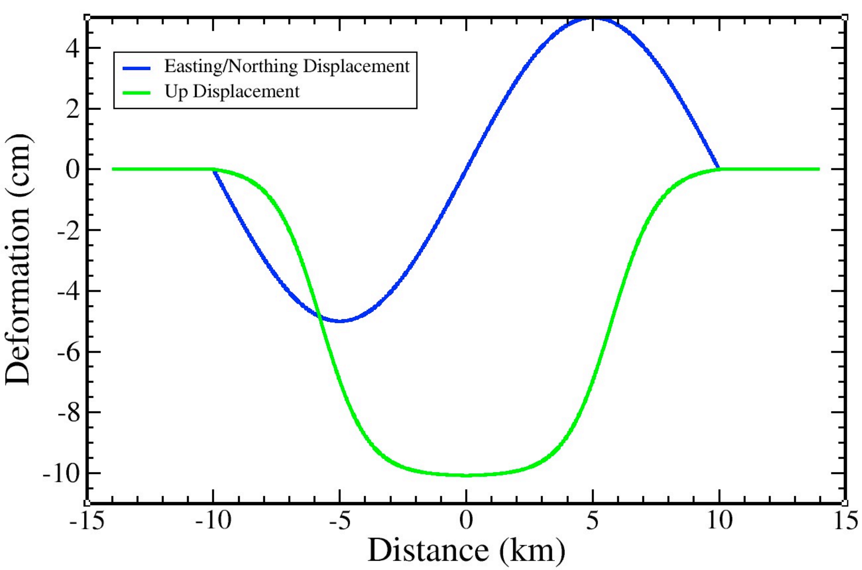

Subsidence Bowl Deformation

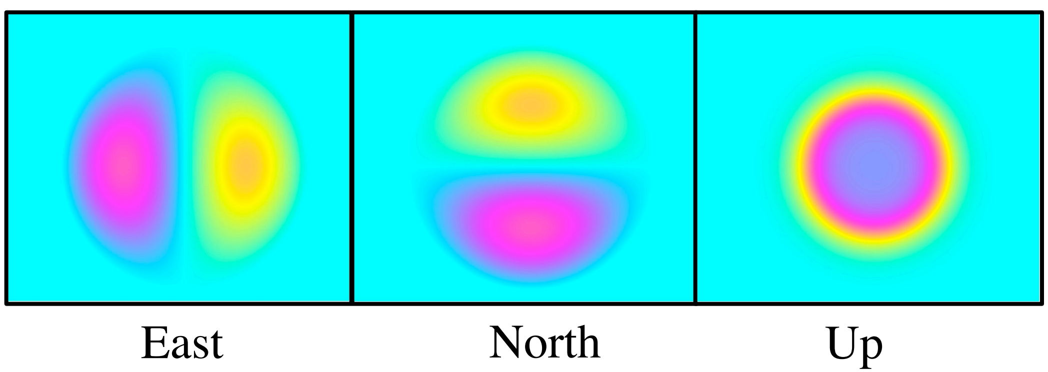

12 cm color wrap

Simulation Results

- Results of the inversion for the subsidence bowl assuming a 0.92 interferometric correlation. Precision results follow the model.

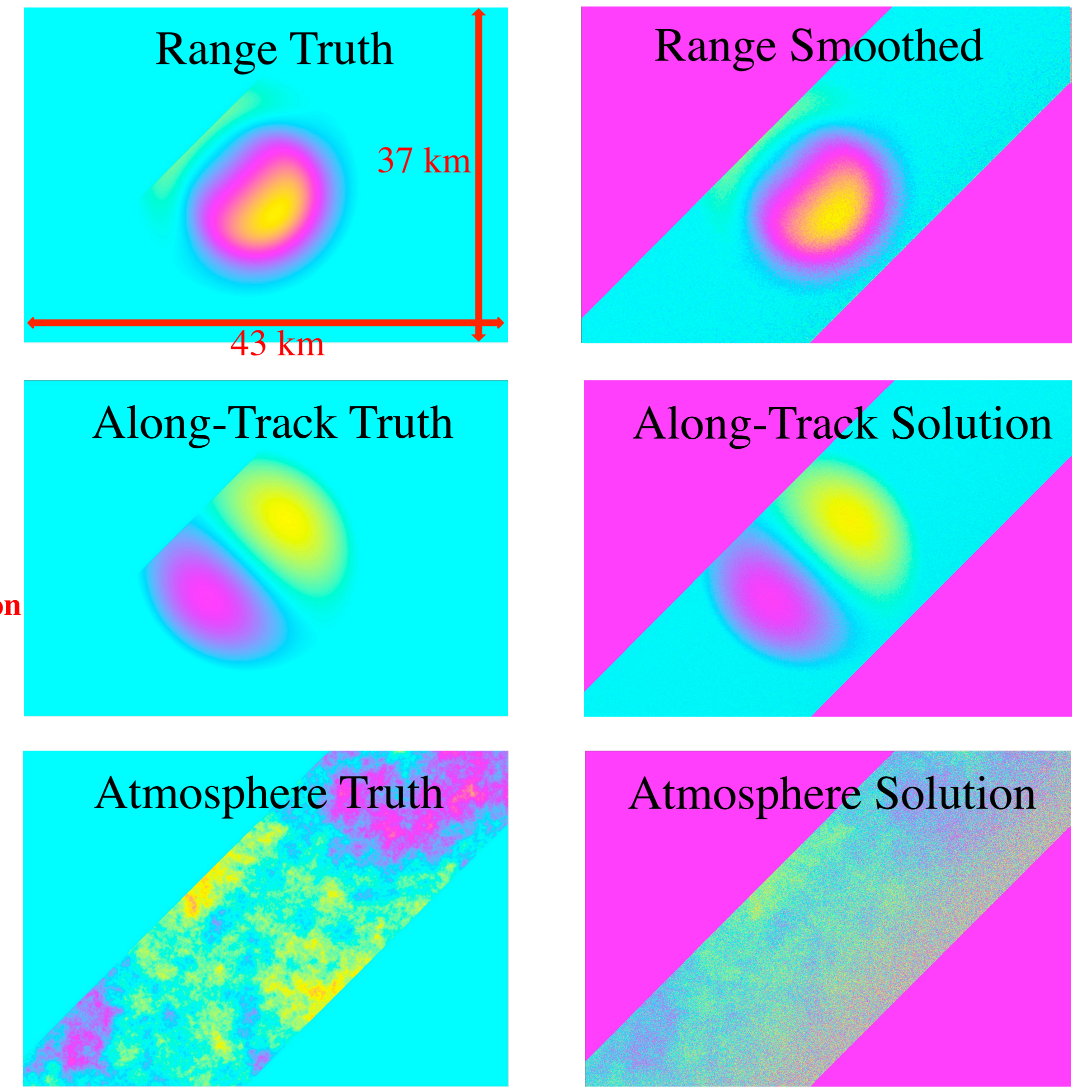

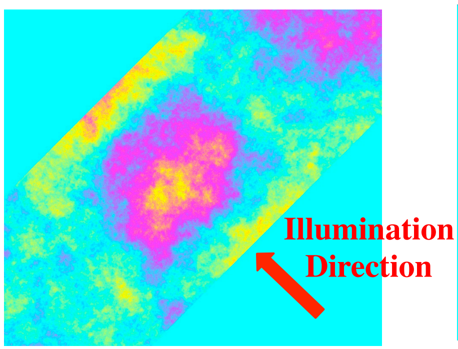

Broadside
Line-of-Sight
Measurement

Magnitude and Correlation for $\theta_{az}=0°$

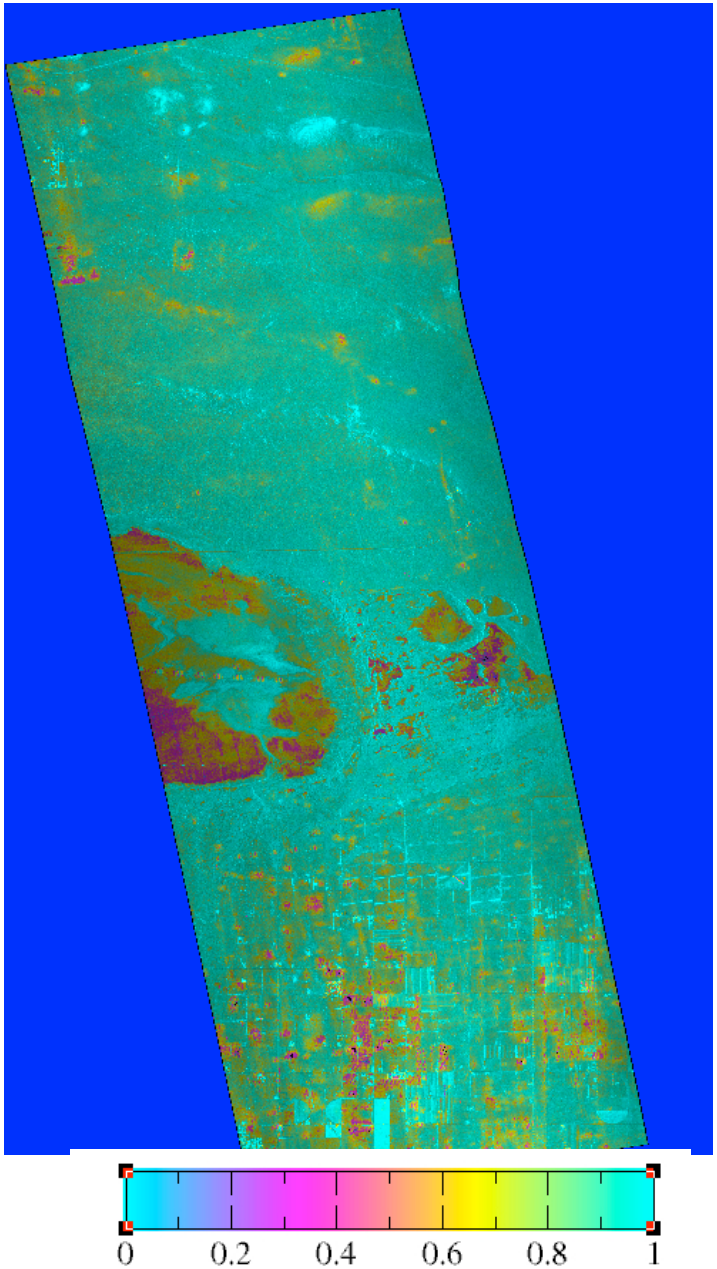

- UAVSAR collected three passes of fully polarimetric multi-squint data with an azimuth steering angle of ±15°.
- Data was collected at a heading of 350° at the UAVSAR nominal flying altitude of 12.5 km over the Rosamond Dry Lake Bed calibration site in California.
- Region is located in Mojave Desert with a urban area in southern section of the scene.
- Time interval between multi-squint observations is approximately 20-25 sec.

I

Multi-Squint Interferograms

$s_1 s_2^*$
26.2 min

$s_2 s_3^*$
33.3 min

$s_1 s_3^*$
51.9 min

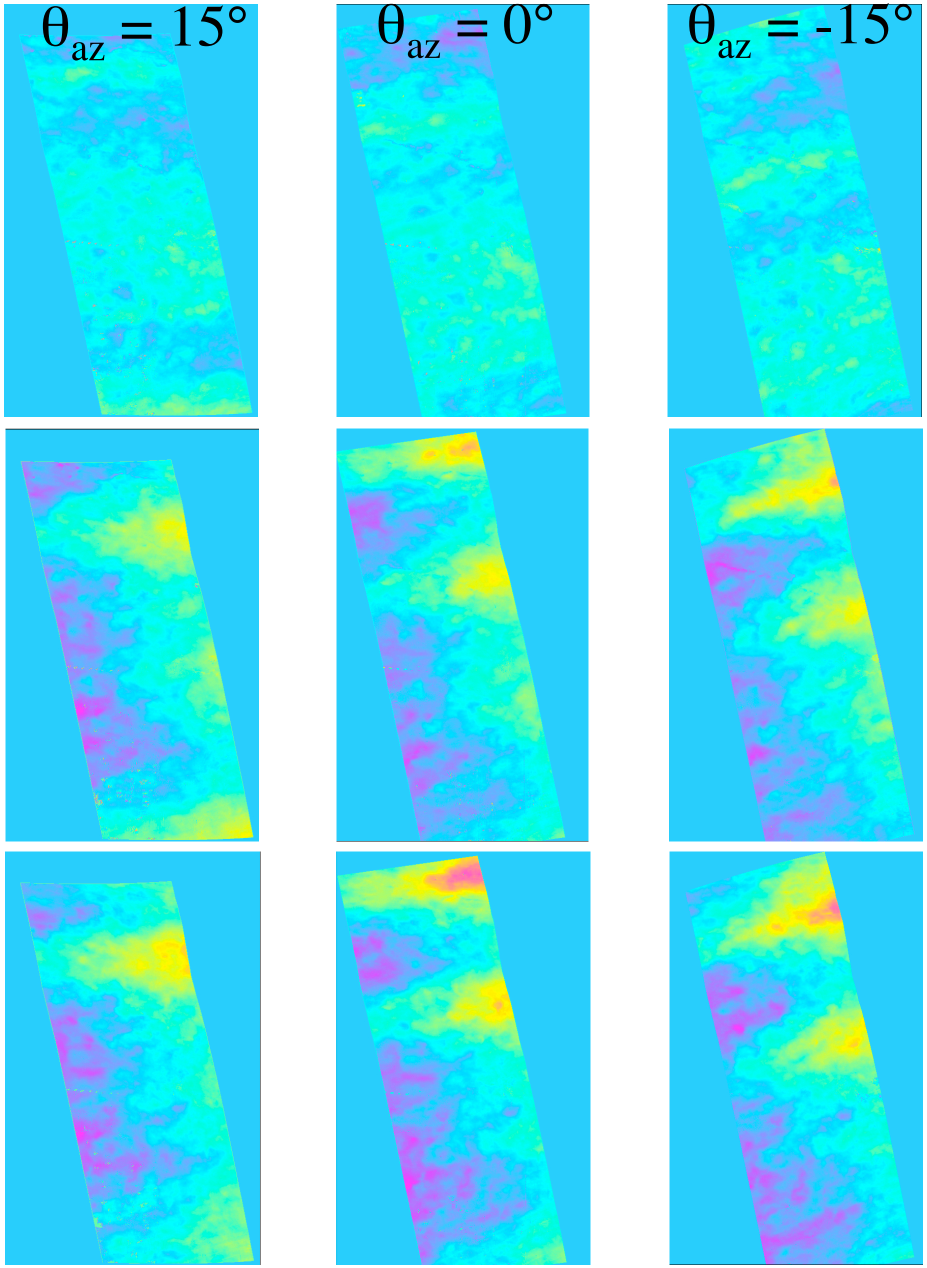

<u>Time Between Passes</u>

1-2 26.2 min
2-3 33.3 min
1-3 51.9 min

Data collected July 10, 2010

Bistatic Observations

Bistatic Observations

- Bistatic observations offer the ability to collect data with:
  - Variable baselines and without temporal decorrelation
  - Repeat pass times from seconds to minute to characterize for short temporal decorrelation of targets
  - Scattering geometries that extend beyond the standard backscatter geometries.

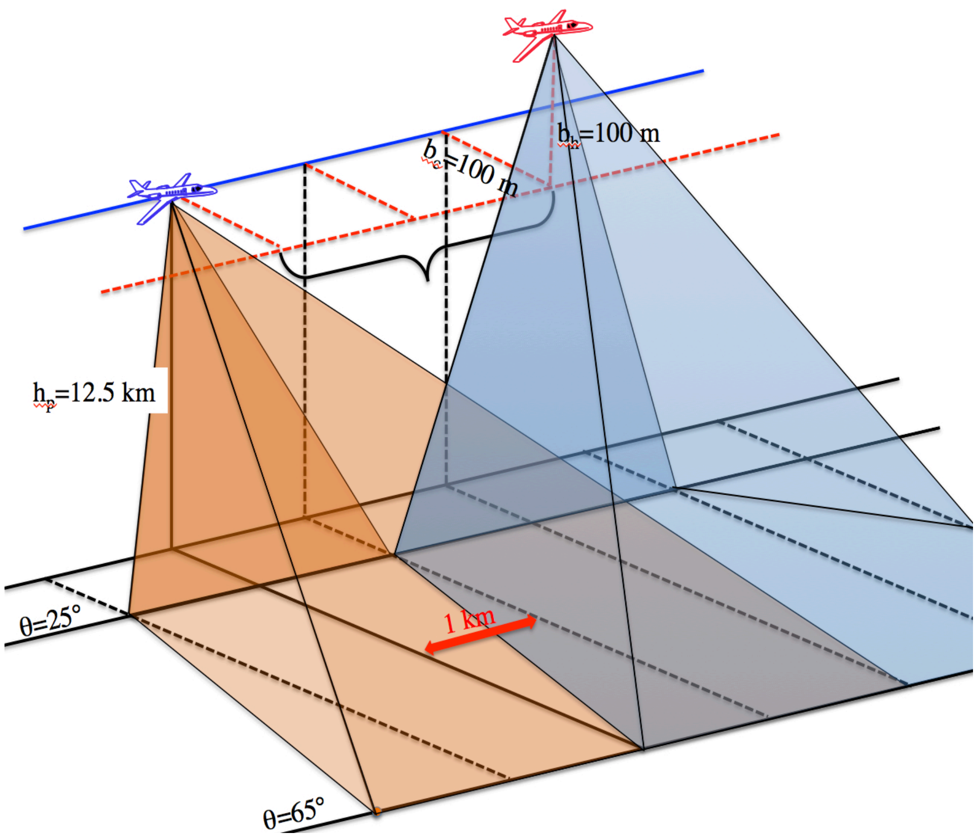

- There are both observational and processing challenges with bistatic observations. Observation challenges include:
  - Determining allowable safe bistatic flying configurations.
  - Assessing which bistatic configurations are viable from a hardware safety and useful signal perspectives.
  - Recording both direct and reflected signals.
  - Maintaining bistatic imaging geometry during flight.

Bistatic Observations

- We have two copies of the UAVSAR radar and two G-III aircraft so we are currently studying bistatic experiment possibilities using two UAVSAR L-band radars.
  - We have also studied doing bistatic observations with other platforms.
- There are a number of processing considerations and modifications needed to handle motion compensation and focusing that are under development.

Spotlight Modes

Spotlight Modes

- Spotlight imaging modes provide a means of obtaining increased azimuth resolution and of providing imagery with continuing vary aspect angle.
  - Use the azimuth beam steering capability to keep the beam pointed at a fixed target or in slewed spotlight mode where the beam velocity is less than the aircraft velocity.
  - Fly is a circular trajectory to stare at a fixed region to obtain continuous aspect angle imaging of a scene.

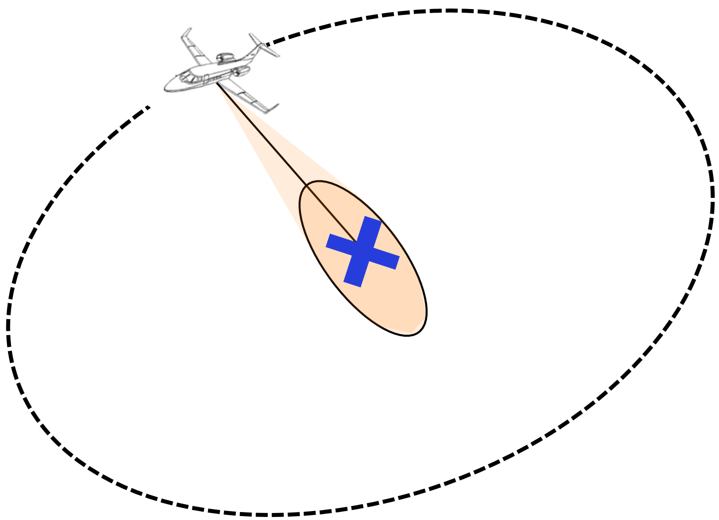

Increased Bandwidth
and
Sampling Frequency

Increased Bandwidth and Sampling Frequency

- The present digital system is limited to a sampling frequency of 180 MHz or and effective range bandwidth of 80 MHz (1.75 m range resolution).
- We are exploring upgrades to the digital system that would allow for increased bandwidth and sampling frequency.
  – This requires both new hardware and software changes to the flight system.

Single-Pass
L-band Interferometry
(Global Hawk)

Single Pass L-band PolInSAR

- One of the goals from the very beginning of the UAVSAR development was to have a single pass L-band PolInSAR system.
- A single pass PolInSAR system would enable polarimetric interferometric observations without temporal correlation issues.
  – Ideal for PolInSAR studies of vegetation and ice sheet or glaciers.
  – Mapping of tree height and bare surface topography valuable for ecosystem, hydrology and other applications.
  – Topography measurements would have same phase center in volume as potential L-band measurements.
  – Useful for testing out potential future tandem satellite L-band algorithms.
- Need a platform with mount points for two antennas with sufficient baseline to have adequate k_z values.
  – Global Hawk flown at appropriate altitudes can support single pass L-band interferometry.

Global Hawk Dual Pod System

- Modify Global Hawk to have to pods mounted on wings to with a 5.5 m baseline housing the active array L-band antenna, INU and GPS antenna.

Tomography

Tomography

- UAVSAR has conducted several non-zero baseline data collections in the US, Panama that have been used for PolInSAR and SAR tomography studies.

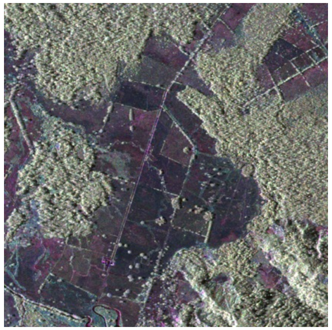

PolinSAR in
La Amistad
National Forest

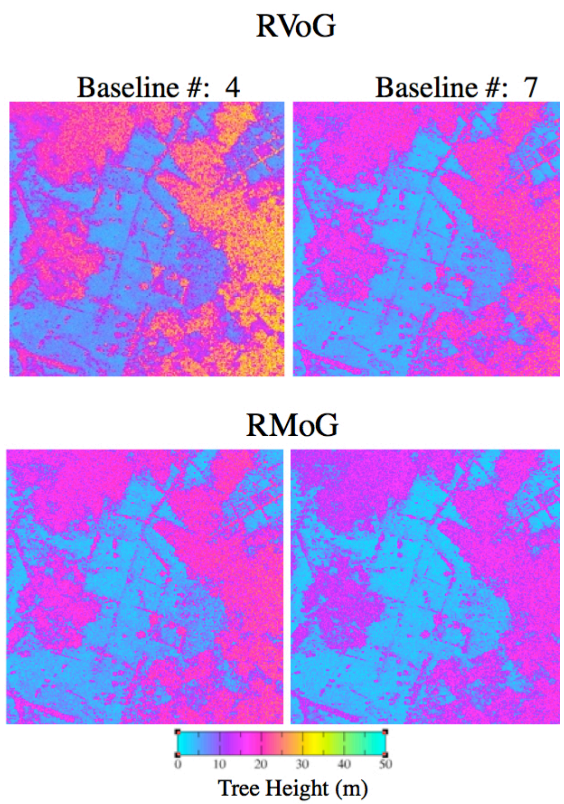

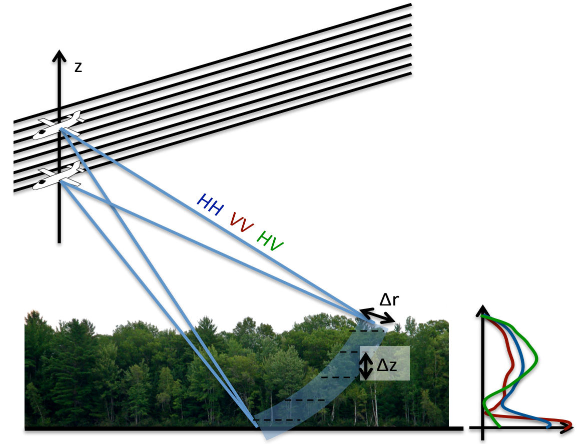

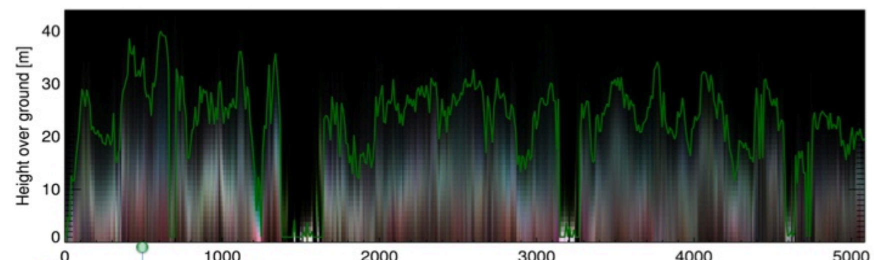

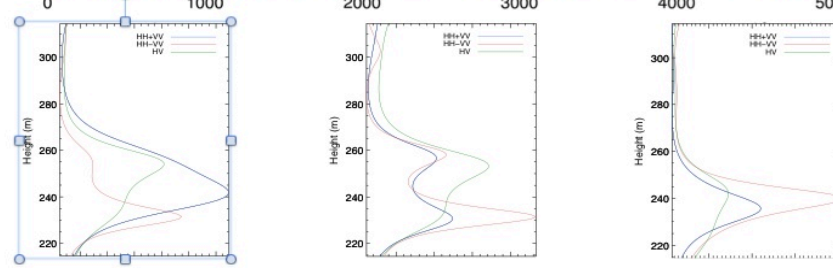

Tomographic profiles obtained in the Harvard forest using data collected from 13 passes in August of 2009 by the L-band UAVSAR instrument.

Tomography Collections

- UAVSAR has made limited collections suitable for tomographic observations. Recently we have added several collections in Germany and Gabon, Africa suitable for tomographic experiments.
- Data in Gabon will be collected on multiple dates suitable for multi-temporal tomographic studies.
- Data in Germany is collected with two different baseline configurations for the Traunstein Forest and over Munich City for urban studies.

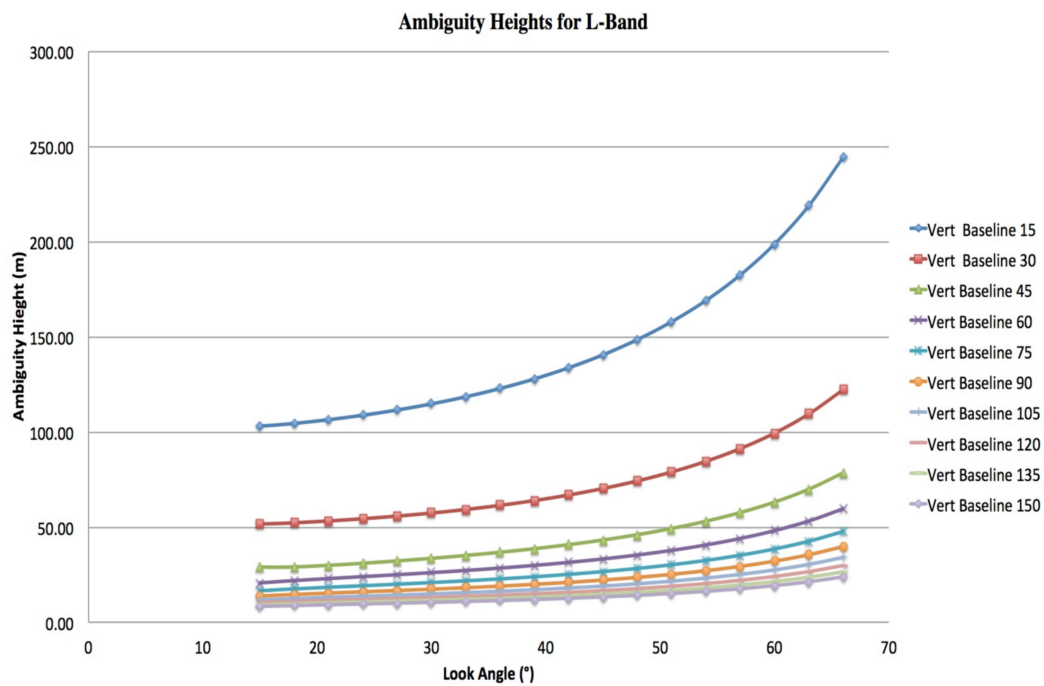

Germany Lines

- UAVSAR collected both multi-squint and tomographic lines at Traunstein and Munich.

Munich

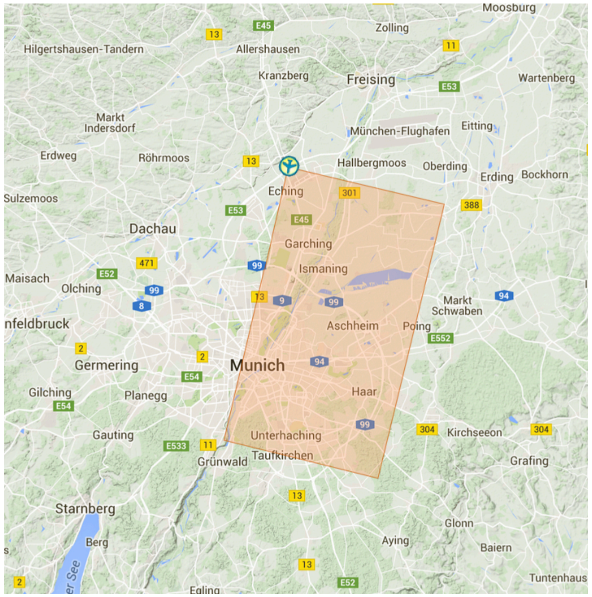

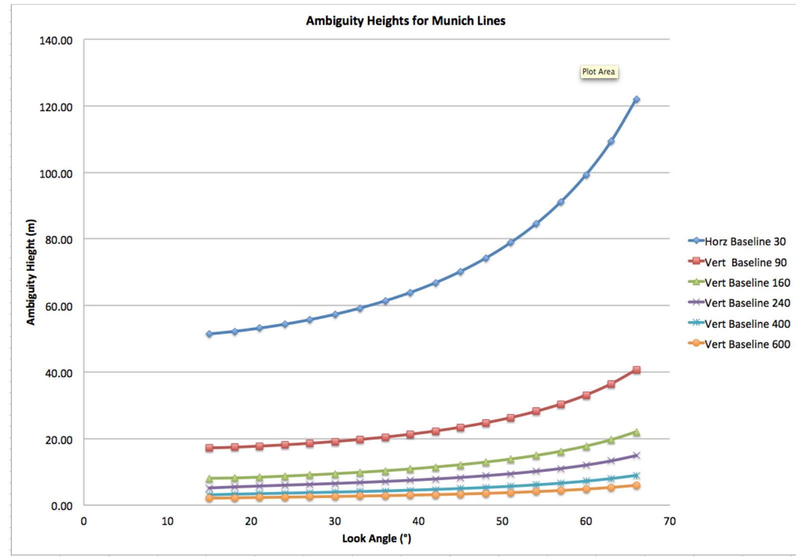

Traunstein

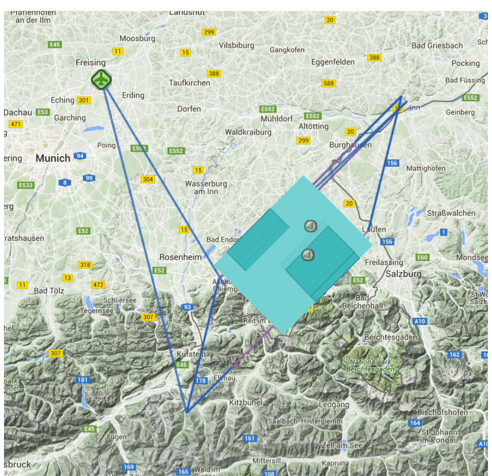

- Developing stack products with non-zero and large baselines with associated ancillary files (e.g., k_z) needed to process the data.

Backup

Mathematical Formulation

- Interferometric phase measurements, ϕ_i, obtained from multiple squint angles with line-of-sight vectors, $\hat{\ell}_i$, i=-1,0,1

$$\phi_i = \frac{4\pi}{\lambda}\left[\langle \vec{d}, \hat{\ell}_i \rangle + \frac{\Delta\rho_{atm}}{cos\theta_{sq}}\right]$$

where

$$\vec{d} = \left[\begin{array}{ccc} d_\rho & d_s & d_\perp \end{array}\right]$$

$$\begin{aligned} \hat{\ell}_{-1} &= \cos\theta_{sq}\hat{\rho} - \sin\theta_{sq}\hat{s} \\ \hat{\ell}_0 &= \hat{\rho} \\ \hat{\ell}_1 &= \cos\theta_{sq}\hat{\rho} + \sin\theta_{sq}\hat{s} \end{aligned}$$

- These observations can been written in matrix form as

$$\vec{\phi} = \frac{4\pi}{\lambda} A\vec{D}$$

where

$$A = \left[\begin{array}{ccc} \cos\theta_{sq} & -\sin\theta_{sq} & \frac{1}{\cos\theta_{sq}} \\ 1 & 0 & 1 \\ \cos\theta_{sq} & \sin\theta_{sq} & \frac{1}{\cos\theta_{sq}} \end{array}\right] \qquad \vec{D} = \left[\begin{array}{ccc} d_\rho & d_s & \Delta\rho_{atm} \end{array}\right]$$

Solution Vector

- The solution vector to the multi-squint equations is given by

$$\vec{D} = \begin{bmatrix} d_\rho \\ d_s \\ d_{atm} \end{bmatrix} = \begin{bmatrix} \frac{1}{4}\frac{(5+\cos(2\theta_{sq}))d_{-1}}{\sin^4\theta_{sq}} - \frac{3}{2}\frac{d_1}{\tan^2\theta_{sq}\sin^2\theta_{sq}} \\ \frac{1}{2}\frac{d_0}{\sin^2\theta_{sq}} \\ -\frac{3}{2}\frac{d_{-1}}{\tan^2\theta_{sq}\sin^2\theta_{sq}} + \frac{1}{2}\frac{(2+\cos(2\theta_{sq}))d_1}{\tan^2\theta_{sq}\sin^2\theta_{sq}} \end{bmatrix}$$

where $d_i=(1/4\pi)\phi_i$ are the line-of-sight displacements derived from the phase measurements.

- The line-of-sight vector can be written in the form

$$\hat{\ell} = \begin{bmatrix} \sin\theta_\ell \sin\theta_{az} \\ \sin\theta_\ell \cos\theta_{az} \\ -\cos\theta_\ell \end{bmatrix}$$

- The squinted looked angle, θ_ℓ , as function of the broadside look angle, θ_{ℓ_o}, is given by

$$\tan\theta_\ell = \frac{\tan\theta_{\ell_o}}{\cos\theta_{az}}$$

and the cosine of the squint angle given by

$$\cos\theta_{sq} = \sin\theta_\ell \sin\theta_{\ell_o}\cos\theta_{az} + \cos\theta_\ell\cos\theta_{\ell_o}$$

Covariance Matrix

- The covariance matrix for the least squares solution is given by

$$cov_{\vec{D}} = \left[A^t Q^{-1} A\right]^{-1}$$

where Q is the covariance matrix of the observations given by

$$Q = \frac{\lambda}{4\pi} \frac{1}{\sqrt{2N_L}} \sqrt{\frac{1-\gamma^2}{\gamma^2}} \begin{bmatrix} 1 & 0 & 0 \\ 0 & 1 & 0 \\ 0 & 0 & 1 \end{bmatrix}$$

where γ is the interferometric correlation and N_L is the number of looks.

- Explicitly, the covariance matrix is

$$cov_{\vec{D}} = \left(\frac{\lambda}{4\pi}\right)^2 \frac{1}{2N_L} \frac{1-\gamma^2}{\gamma^2} \begin{bmatrix} \frac{1}{4}\frac{5+\cos(2\theta_{sq})}{\sin^4(\theta_{sq})} & 0 & -\frac{3}{2}\frac{\cot^2(\theta_{sq})}{\sin^2(\theta_{sq})} \\ 0 & \frac{1}{2\sin^2(\theta_{sq})} & 0 \\ -\frac{3}{2}\frac{\cot^2(\theta_{sq})}{\sin^2(\theta_{sq})} & 0 & \frac{1}{2}\frac{(2+\cos(2\theta_{sq}))\cot^2(\theta_{sq})}{\sin^2(\theta_{sq})} \end{bmatrix}$$